

Improving initial-state-dependent quantum circuit optimization by introducing state labels

Toshiaki Kaji, Koji Terashi, and Ryu Sawada

International Center for Elementary Particle Physics (ICEPP), The University of Tokyo, 7-3-1 Hongo, Bunkyo-ku, Tokyo 113-0033, Japan

While the capabilities of quantum hardware have significantly advanced in recent years, executing quantum algorithms as quantum circuits at the lowest possible cost remains crucial, regardless of the hardware progress. We are developing a quantum-state-dependent circuit optimizer called AQCEL. Our guiding principle, implemented as the AQCEL optimization protocol, is to optimize quantum circuits by measuring the states of the control qubits to identify and eliminate unnecessary control operations. In this paper, we introduce two key improvements: the state label manager that reduces unnecessary state measurements and the CX -pair removal process that eliminates redundant gate pairs. These enhancements significantly reduce the number of two-qubit gates, improving the fidelity of quantum circuits executed on quantum hardware. To demonstrate the effectiveness of our method, we apply AQCEL to quantum circuits for the quantum parton shower algorithm. Experimental results using the IBM quantum computer show a substantial reduction in gate counts and an improvement in fidelity compared to the conventional optimization technique as well as the original AQCEL protocol. Our findings highlight the potential of state-dependent circuit optimization for enhancing the performance of quantum algorithms on near-term quantum devices.

1 Introduction

Among fields of fundamental science, high-energy physics has benefited from advanced computing

Toshiaki Kaji: kaji@icepp.s.u-tokyo.ac.jp

techniques. Understanding the static and dynamical properties of fundamental constituents in nature such as quarks and leptons requires large computational resources, motivating the development of new computational tools. Quantum computing is emerging as a leading technology for the next computing paradigm and has the potential for transformative changes in various fields including high-energy physics. Numerous studies are already underway, both experimental and theoretical, exploring the use of quantum computers in high-energy physics [1–12].

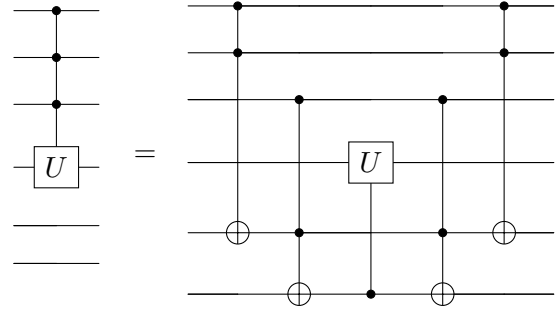
However, the present quantum computers with non-negligible hardware noise and technical constraints pose challenges to effective executions of quantum algorithms. Quantum operations including quantum gates and measurements induce errors due to finite operational accuracy. Therefore, it is essential to implement quantum algorithms using fewer quantum gates to minimize overall gate errors. The circuit synthesis and optimization techniques to implement quantum algorithms with fewer number of gates are actively investigated [13–22]. Various error mitigation techniques to reduce the impact of noise have also been proposed in literatures and investigated with quantum hardware [23–30]. The combination of these techniques is crucial for enhancing the performance of quantum computers.

Two-qubit entangling gates, such as the controlled-NOT (CNOT) gates, often dominate gate errors. Additionally, identifying an efficient qubit mapping to the physical layout of quantum hardware is crucial, especially in systems with limited qubit connectivity. Poor mapping would result in an increased number of SWAP gates, which in turn leads to a higher number of CNOT gates after decomposition. Therefore, one of the primary challenges in quantum circuit optimization is to minimize the number of two-qubit gates, as they contribute significantly to overall

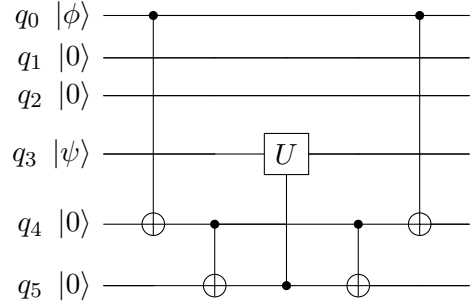
error rates. If the quantum circuit is designed to work with various initial states, some of the operators may become trivial when the circuit is executed with specific initial states. Therefore, an initial-state-dependent optimization method can reduce unnecessary controlled operations more aggressively compared to traditional circuit optimization techniques that usually maintain the equivalence of the quantum circuit for any inputs. The Relaxed Peephole Optimization (RPO) [15] accounts for quantum states to reduce control operations in specific conditions. However, this method does not work when qubits are entangled. Another method, the ZX-calculus [16], has successfully summarized general rules of graphical expression and simplification for a quantum circuit. Quantum operations can be represented using diagrams made up of colored spiders connected by wires. The copy rule or Hopf rule allows for the graphical elimination of wires between qubits, which reduces redundant entangling operations. As a result, the circuit depth can be shortened. While it is effective for a wide range of quantum circuits, it cannot remove all redundant entangling operations in polynomial time.

To address this issue, we introduced AQCEL (*Advancing Quantum Circuit by ICEPP and LBNL*), an initial-state-dependent optimizer for quantum circuits. The key concept of AQCEL optimization is to remove gates from the circuit in polynomial time by focusing on the equivalence of the final states in the circuit, not the circuit itself, before and after the optimization. This is in stark contrast to traditional circuit optimization techniques that maintain the equivalence of the quantum circuit. In order to realize this, AQCEL identifies and removes redundant control operations based on the quantum states of control qubits just before the controlled operators act on those qubits. Therefore, AQCEL-optimized circuits vary depending on the initial states, while preserving the essential functions of the circuit computation.

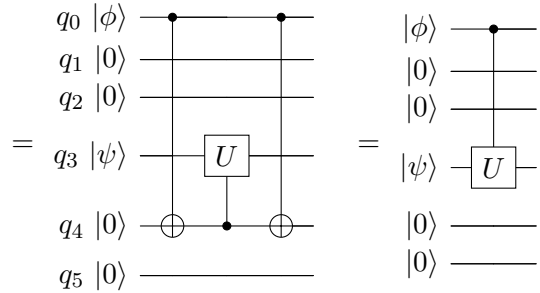
AQCEL performs the measurements every time it encounters controlled operators in the circuit to identify the redundancy of the gate. However, if the states of the control qubits are known from the earlier measurement in the circuit or selection of the initial states, one can avoid another measurement to save the execution time on quantum hardware in the optimization.



(a) Decomposition of a multi-qubit controlled operator



(b) Removal of redundant control operations



(c) Removal of redundant CX pairs

Figure 1: Example of how redundant CX pairs appear and how to remove them. (a) AQCEL will decompose a multi-qubit controlled operator into $RCCX$ gates (illustrated as CCX gates in the figure) and a single controlled- U gate. (b) AQCEL can eliminate redundant control operations depending on the states of qubits. (c) Redundant CX pairs can be removed once they are identified as redundant.

Furthermore, it turns out that AQCEL can be improved to further remove redundant CX gates that appear in certain conditions. First, AQCEL decomposes multi-controlled operators, before the measurements of control qubits, into a set of $RCCX$ (relative phase Toffoli) gates and a singly-controlled unitary gate by adding ancilla qubits, as shown in Figure 1(a). This decomposition is crucial for performing the entire optimization process in polynomial time, otherwise the identification of redundant control operations re-

quires exponential cost due to the number of basis states increasing as 2^n with n control qubits. Note that after the decomposition, the *RCCX* gates appear as pairs in a reverse order before and after the controlled- U gate. We refer to this pairing of *RCCX* gates as *RCCX* pair in the following (similarly for the *CX* pair). Then, at most two qubits are measured at a time for each *RCCX* gate. Consider the case in which the AQCEL optimizes the decomposed circuit with the initial state shown in Figure 1(b), where $|\phi\rangle$ and $|\psi\rangle$ are arbitrary states. In this case, one of two control operations can be removed from every *RCCX* gate. This identification and removal of redundant control operations is an essential function that the AQCEL provides. The remaining *CX* gates are redundant, but they still remain. Once these redundant *CX* pairs can be identified, they can be removed by truncating the sequence of control-target qubit operations from q_0 to q_4 and q_5 , as shown in Figure 1(c). First, the *CX* pairs on the qubits q_4 - q_5 are removed, and the control of the U gate is moved from q_5 to q_4 . Then, the *CX* pairs on the qubits q_0 - q_4 are removed, and the control of the U gate is moved from q_4 to q_0 . Since the *CX* gates increase circuit depth and accumulate gate errors, the removal of such redundant *CX* pairs would improve the circuit performance.

In this paper, we present two key enhancements to the AQCEL protocol: (1) the state label manager, which remembers the labels that represent quantum states of qubits to minimize unnecessary measurements, and enables us to implement (2) the removal of redundant *CX* pairs. These improvements enable more effective optimization by reducing the number of two-qubit gates, ultimately enhancing the fidelity of quantum computations. To evaluate the performance of enhanced AQCEL optimizer, we apply AQCEL to the quantum parton shower (QPS) algorithm, a quantum computing-based simulation of high-energy particle reactions. Using both simulator and real quantum hardware experiments, we demonstrate that our optimization techniques lead to a significant reduction in gate counts and an improvement in computational accuracy.

The remainder of this paper is organized as follows: Section 2 provides an overview of the AQCEL protocol and its original optimization techniques. Section 3 details the newly introduced

functions called state label manager and the *CX*-pair removal method. Section 4 introduces the QPS algorithm for the benchmark and the experimental setup. Section 5 presents the benchmark results of the improved AQCEL protocol against the QPS circuits with quantum hardware. Section 6 concludes with discussion of the implications and future directions for state-dependent quantum circuit optimization. Finally, Section 7 summarizes the content of this paper.

2 Overview of previous AQCEL

AQCEL is an initial-state-dependent optimizer for a quantum circuit. If a quantum circuit is designed to work with different initial states, redundant gates may appear once the specific initial state is chosen. In this case, AQCEL can identify redundant gates depending on the states of qubits. While AQCEL may not always maintain circuit equivalence, it can significantly reduce the number of redundant gates in a specific situation. This section provides an overview of AQCEL’s functionality.

AQCEL was introduced for the first time in Ref. [31], and we refer to the version in Ref. [31] as AQCEL-v1 in this paper. First, AQCEL attempts to decompose a multi-qubit controlled- U gate into relative phase Toffoli gates [32] called Margolus gates or *RCCX* gates and a single controlled- U gate. Then, AQCEL removes obviously-redundant gate pairs such as those satisfying $UU^\dagger = I$. The most essential function is the removal of redundant control operations. For every controlled operator, AQCEL measures the states of control qubits in the Z basis. Thanks to the decomposition of multi-qubit controlled operators, the measurements are performed for only up to two qubits. Here the measurement is performed with statistical sampling of the qubit states, and a single-shot or mid-circuit measurements is not considered. This strategy should work for any number of controlled qubits. AQCEL controls a noise threshold parameter, and if the measured probability of a given computational basis state is lower than the threshold, that state is ignored. Depending on the measured outcome of control qubits, AQCEL replaces the controlled operator with a less-costly operator. For example, when the state of two control qubits is a superposition of $|00\rangle$, $|01\rangle$, and $|11\rangle$, we

can remove the control operation from the rightmost qubit, replacing the CCX or $RCCX$ gate with a CX gate. When the control operation is removed from the first $RCCX$ gate of the pair produced in the decomposition (see Figure 1(a)), the second $RCCX$ gate of the pair can be also replaced according to the optimization result of the first $RCCX$ gate. The higher the noise threshold becomes, the stronger the reduction of the control operations, hence the less equivalent the optimized circuit to the original one. The reduction of noisy control operations is a benefit, but the trade-off is the inaccuracy of the resulting circuit. Therefore, the optimal threshold needs to be determined separately for each quantum circuit. Classical calculation requires an exponential resource to identify zero- or low-amplitude computational basis states. The AQCEL can identify such states and optimize a quantum circuit in polynomial time by utilizing the gate decomposition and quantum measurements, making it practically applicable to quantum circuits composed of a large number of qubits.

3 Improvements in AQCEL

AQCEL-v1 performs the repeated measurements as many times as the number of controlled operators in the circuit. However, this feature may result in consuming more resources of quantum computers than necessary. In addition, AQCEL-v1 leaves redundant CX gates in specific conditions even after the optimization, as illustrated above. To improve these features, we implement a function called the state label manager, which saves the minimum information of qubits required to determine whether to perform a state measurement. With this function, the AQCEL manages to further identify redundant CX gates for removal. The implementation of the state label manager and the removal of redundant CX pairs is the main improvements described in this paper, and the improved AQCEL with these functionalities is referred to as AQCEL-v2. This section describes how these features are implemented.

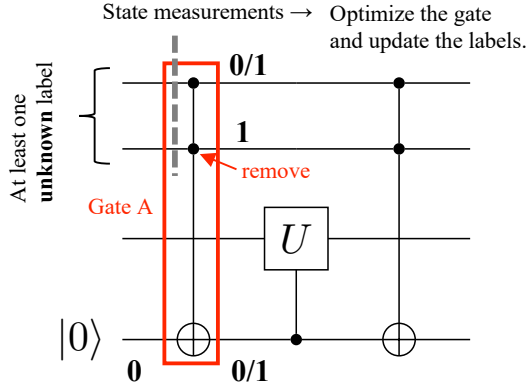
3.1 State label manager

AQCEL needs to know the states of control qubits every time it encounters controlled operators in the circuit. However, the qubit state is sometimes

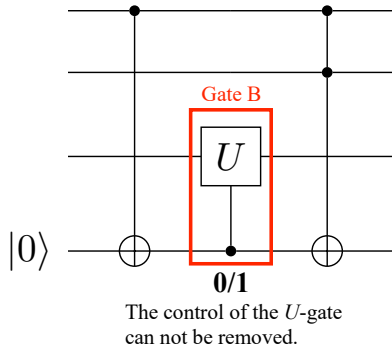
obvious, in which case the measurement is unnecessary. A typical scenario is the case where the previously-measured qubit states are unchanged when they are acted on by another operator. Of course, it is not feasible to remember the entire set of qubit states and track them efficiently due to the limitations of classical memory. However, it is tractable to keep the minimum information about qubits as *labels*, such as whether they are $|0\rangle$ or $|1\rangle$ states, or a superposition of them. If the qubit state is a superposition state, it is most likely that the control operation on that qubit cannot be removed.

The states of each qubit are managed with five labels: **0**, **1**, **Bell**, **0/1**, and **unknown** (denoted by bold letters). The **0** and **1** stand for the states $|0\rangle$ and $|1\rangle$, respectively. The **Bell** indicates that this qubit is making a state like $\alpha|00\rangle + \beta|11\rangle$ or $\alpha|01\rangle + \beta|10\rangle$ with other qubits. For the **Bell** label, we manage to remember the parities of each qubit, whether it forms the state like $\alpha|00\rangle + \beta|11\rangle$ or $\alpha|01\rangle + \beta|10\rangle$. If several qubits are assigned **Bell** labels independently, it is not obvious whether they are entangled with each other, therefore, the parities of each qubit should be remembered as different **Bell** groups. If other qubits are found to belong to the existing **Bell** group, these qubits are added to the **Bell** group. Therefore, it is possible that each **Bell** group has more than two qubits. The state, which is a superposition of $|0\rangle$ and $|1\rangle$ but not labeled as **Bell**, is labeled as **0/1**. The **unknown** indicates that this qubit state is unknown and needs to be measured for the redundant control operation removal as usual. To conserve memory resources, the entanglement with other qubits, except for the **Bell** group, and the amplitude of each state are not monitored in this state label manager.

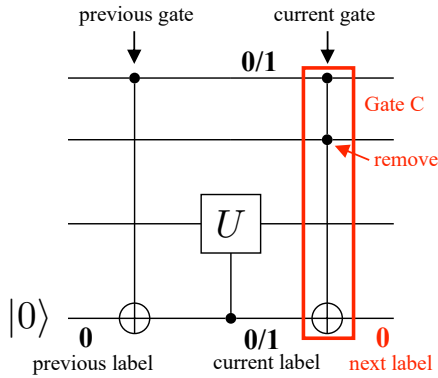
Since all the qubits are initialized to $|0\rangle$ state at the beginning of circuits, the labels are also initialized to **0**. An obvious state change like $|0\rangle$ to $|1\rangle$ by Pauli X operator updates the label from **0** to **1**. The X operator also flips the parity of **Bell** qubits. If the CX gate is applied to the control qubit labeled as **Bell** and the target qubit as **0**, the label of the target becomes **Bell** in the same group and the same parity as the control qubit. Other operators change the qubit labels to **unknown**. If at least one of the control qubits has **unknown**, the state measurement is



(a) First gate(Gate A): Optimization of the $(R)CCX$ gate with **unknown** label



(b) Second gate(Gate B): Judgment of the optimization without measurements



(c) Third gate(Gate C): Control operation removal without state measurements

Figure 2: Example of the workflow of the optimization and state labeling. (a) State measurements are performed to identify redundant control operations at the first gate, denoted as gate A. From the measurements, the gate is replaced by a CX gate, and the labels of the control and target qubits are updated. (b) Since the label of the control qubit is $0/1$ in the second gate denoted as gate B, we can identify that this control operation is necessary and cannot be removed. (c) Since the gate C is paired with the gate A, it is replaced by a CX gate as for the gate A. In addition, the state of the target qubit should return to the 0 state.

performed. Once the state measurement is performed, the states of the control qubits become known and their labels are updated to anything other than **unknown**. AQCEL also performs the state measurement when the gate has two control qubits, both labeled **Bell** or $0/1$, because some control operations could be removed in this case. For example, if the labels of the two control qubits are $0/1$, it is possible for the quantum state to be something like $\alpha|00\rangle + \beta|01\rangle + \gamma|11\rangle$, in which case one of the control operations can be removed. Similarly, if one label is **Bell** and the other is $0/1$, the control operations can be removed if the measurements find that they belong to the same **Bell** group. If the labels of the two control qubits are **Bell** and we already know they belong to the same group, we can skip the state measurements of the control qubits.

Figure 2 shows an example of how the optimization performs and the labels are recorded. (a) Consider the case where at least one of the control qubits is labelled as **unknown** at the $(R)CCX$ gate denoted as gate A, therefore the control qubits are measured. We assume that the labels of the first and second control qubits turn out to be, e.g., $0/1$ and 1 , respectively, from the measurements. In this case, the control operation of the second qubit is redundant, and the $R(CCX)$ gate can be replaced by the CX gate. If the state of the target qubit is 0 at the CX gate, the label of the control qubit propagates to the target qubit, making the target label $0/1$ as well. (b) Since the control qubit of the controlled- U gate denoted as gate B is now $0/1$, this control operation needs to be kept as it is, eliminating the need of the measurement. (c) The gate C ($(R)CCX$ gate) is the same as the gate A. The state of the target qubit remains unchanged between the gate A and C, therefore the gate C is replaced by a CX gate as for the gate A. Furthermore, in this case, the label of the target qubit reverts to its original label before the gate A is applied. To identify when the qubit label can be reverted, we record what gate is applied to the qubit previously in time relative to the current gate, and the corresponding previous label of the qubit state, as illustrated in Figure 2(c). For instance, in the case of gate C as the current gate, the gate A is recorded as the previous gate because it is the last gate applied to the same target qubit before the gate C. From the

previous label $\mathbf{0}$ of the target qubit, the label of the qubit is reverted to $\mathbf{0}$ after the current gate of gate C. Practically, this situation often occurs when a multi-controlled gate is decomposed by adding ancilla qubits because the labels of ancillae should always return to $\mathbf{0}$. This functionality is necessary to implement the feature that identifies and removes redundant CX pairs, introduced in the following subsection.

3.2 Removal of redundant CX pairs

AQCEL makes the $RCCX$ gate pairs by decomposing a multi-qubit controlled gate as discussed above. If one of the $RCCX$ control operation is removed as redundant operation, then the CX pair remains. In most cases, the original state of the target qubit of the CX gate is $|0\rangle$ because it is most likely added as an ancilla in the decomposition of a multi-qubit controlled operator. In this case, the CX pair is redundant and can be removed, as shown in Figure 1(c).

The redundant CX -pair removal is performed as follows. First, we attempt to find a CX pair in the circuit. Once it is found, we determine whether the CX -pair removal is applicable by exploiting the state label manager that monitors the qubit states, introduced in the previous subsection. If the original state of the target qubit of the CX pair is $|0\rangle$ and the state does not change between the CX pair, the CX -pair removal can be applied. As in Figure 1(c), if there is a controlled- U gate in-between the CX pair and the control of the U gate is the same as the target of the CX gates, then the U gate is changed to be controlled by the control of the CX gates and the CX pair is removed.

4 Application to quantum algorithm

To evaluate the performance of the optimization protocol, we apply AQCEL to the quantum circuits of the parton shower algorithm [7]. In this section, we provide a brief description of the quantum circuits and details of the experimental setup.

4.1 Quantum parton shower algorithm

Elementary particle physics is described by quantum field theory, and high-energy physics is one

of the most attractive domains for the applications of quantum computation [8]. For example, strongly interacting non-perturbative phenomena in quantum chromodynamics are hard to simulate classically, resulting in non-negligible theoretical uncertainty when comparing with experimental data. It is known that certain types of quantum dynamics can be efficiently simulated using quantum computer. A quantum algorithm for simulating parton showers (QPS) introduced in Ref. [7] is one such example, enabling parton shower simulation using only polynomial resources. Later, the QPS algorithm was improved [33] to enable kinematical properties using mid-circuit measurements and classical feed-forward. Our study is based on the original QPS algorithm.

This QPS model consists of two types of fermions f_1 and f_2 with corresponding antifermions \bar{f}_1 and \bar{f}_2 and one scalar boson ϕ [34]. Each particle is encoded into 3 qubits to represent their states. There are three parameters of coupling constant g_1 , g_2 , and g_{12} that control the interaction strengths between $f_1(\bar{f}_1)$ and ϕ , $f_2(\bar{f}_2)$ and ϕ , and $f_1\bar{f}_2(\bar{f}_1f_2)$ and ϕ , respectively. The evolution of parton showers is simulated by repeating emission ($f \rightarrow f\phi$) and splitting ($\phi \rightarrow f\bar{f}$) processes by N_{evol} times. The final states of particles are represented by $3(N_{\text{evol}} + 1)$ qubits when initiating a shower with a single particle.

The original QPS paper [7] presented the results simulated on quantum hardware for the shower with $N_{\text{evol}} = 4$ but excluding the $\phi \rightarrow f\bar{f}$ processes to simplify the circuit. For the shower processes without $\phi \rightarrow f\bar{f}$, the fermion state can be represented by a single qubit. Since only scalar-boson emission can occur during the evolution processes, only one additional qubit is required for each step to identify whether the emission of ϕ occurs or not. Therefore, the required total number of qubits and two-qubit gates is $N_{\text{evol}} + 1$ and $2N_{\text{evol}}$, respectively, when the $\phi \rightarrow f\bar{f}$ process is excluded. This is much simpler than the case where the $\phi \rightarrow f\bar{f}$ is included. In this paper, we only treat the full showering processes including $\phi \rightarrow f\bar{f}$. The actual quantum circuit for $N_{\text{evol}} = 1$ with the initial state consisting only of a single f_1 is shown in Ref. [31]. Figure 3 shows a quantum circuit for $N_{\text{evol}} = 2$ and the same initial state with a single f_1 . For

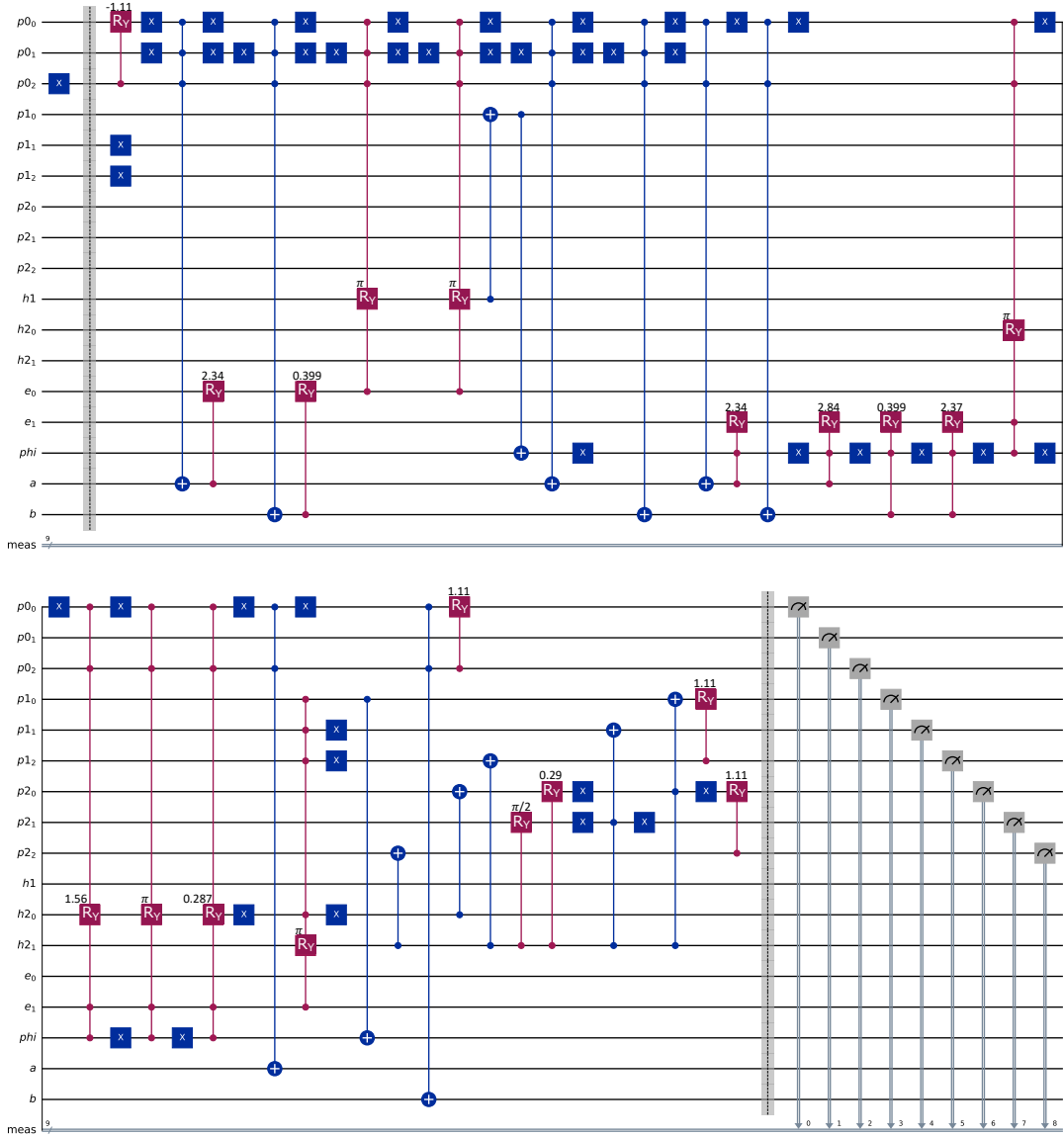


Figure 3: Quantum circuit of the QPS algorithm with $N_{\text{evol}} = 2$. The initial number of particles is one and the state is f_1 . The coupling constants are g_1 , g_2 , and g_{12} . The X operators are shown in dark blue, while the R_y operators are shown in dark red. The number outside the R_y box indicates the rotation angle.

both circuits with $N_{\text{evol}} = 1$ and 2, we assume $g_1 = 2$ and $g_2 = g_{12} = 1$. We use these circuits as a benchmark and refer to them as the 1-step and 2-step circuit, respectively.

4.2 Experimental setup

AQCEL has no functions of quantum circuit transpilation such as qubit mapping to hardware layout or translation into native gates, therefore we use Qiskit [13] for those purposes. The version of each software used in this paper is as follows: Python 3.11.0rc1 [35], Qiskit 1.2.2, Qiskit IBM Runtime 0.30.0, Qiskit Aer 0.15.1, and Mthree 2.7.0 [29]. An ideal output of cir-

cuits is obtained by running a noiseless simulator in Qiskit Aer. To evaluate performance on a real device, we also perform an experiment on the *ibm_fez* backend, which is an IBM quantum computer with a Heron r2 processor of 156 qubits. In the experiment with the real device, a quantum circuit is transpiled with the optimization level 3, and an experiment is performed by using Qiskit Runtime SamplerV2 primitive with the following options: ‘options.experimental = {“skip_transpilation”: True}’, and ‘options.execution.rep_delay = 0.0005’. We apply M3 [29] to mitigate readout measurement errors.

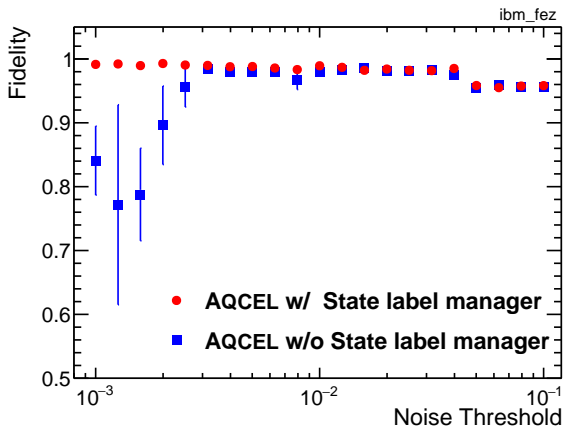


Figure 4: Hellinger fidelity between the distribution of bitstrings measured on the noiseless simulator for the 1-step QPS circuit and measured on the *ibm_fez* backend for the optimized circuit as a function of noise threshold parameter in AQCEL. The red circles and blue squares show the AQCEL with and without the state label manager, respectively.

No other error mitigation techniques are used.¹ The calibration for the M3 mitigation and the experiment with the shower circuit are performed during the same session of Qiskit Runtime. The number of shots is set to 10k times the number of measurement qubits for the M3 calibration, while 100k for each experiment.

If the optimization of circuits is successful, the error rate should decrease, and the output on the real device becomes closer to the ideal output. In order to quantify how close the two outputs are, we use Hellinger fidelity, defined as

$$F = \left(\sum_k \sqrt{p_k^{\text{ideal}} q_k^{\text{opt}}} \right)^2 \quad (1)$$

where p_k^{ideal} and p_k^{opt} are the probabilities of measuring k -th bitstring for the original circuit on the noiseless simulator and for the optimized circuit on the real device, respectively. The index k runs over all the measured bitstrings. This quantity is referred to as fidelity hereafter².

¹We attempted to apply the dynamical decoupling and Pauli twirling techniques to further reduce gate errors, but did not observe any significant improvements in the results. Therefore, these techniques were not used in the final hardware experiments.

²Note that the definition of fidelity used in the present paper is different from the fidelity used in [31].

5 Results

In this section, we present the results of counting the number of two-qubit gates and calculating the fidelity to evaluate the performance of the optimization protocol. In particular, we focus on the improved performance of AQCEL-v2 compared to AQCEL-v1.

The state label manager eliminates the need of repeated measurements for control qubits once they are measured, making this step much faster in AQCEL-v2. The number of measurements required to remove redundant control operations turns out to be reduced from 22 to 3–4 for the 1-step QPS circuit and from 61 to 15–22 for the 2-step QPS circuit depending on the noise threshold ranging between 0.005 and 0.3. The execution time of the optimization is proportional to the number of measurements; for example, the state label manager reduces the execution time of AQCEL-v2 to about 1/7 of AQCEL-v1 for the 1-step QPS circuit.

Figure 4 shows the fidelities for the 1-step QPS circuit optimized by AQCEL with and without the state label manager. When AQCEL performs the removal of redundant control operations on real hardware, sometimes mis-optimization occurs due to errors from finite measurement shots or gate/readout noise. However, since the state label manager records all the labels of the qubits and eliminates the measurements of the control qubits for subsequent gates, such mis-optimizations never occur again. Therefore, the fidelity of the optimized circuit becomes much more stable with the state label manager, as indicated by the red markers, especially in the low threshold region where mis-calibration affects more strongly. The optimized circuit varies significantly in such a low threshold region without the state label manager, therefore, the series of the optimization and the fidelity calculation is performed three times to evaluate the fluctuations of the optimization performances for the noise threshold up to 10^{-2} . Shown in Figure 4 as the blue markers and error bars are the average and root-mean-square of the fidelity values obtained from these samples.

Figure 5(a) shows the 1-step QPS circuit optimized by AQCEL-v1 with the noise threshold = 0.05. The number of CX gates is 115 for the original circuit and it is reduced to 23 by using AQCEL-v1. Each controlled- Ry gate is de-

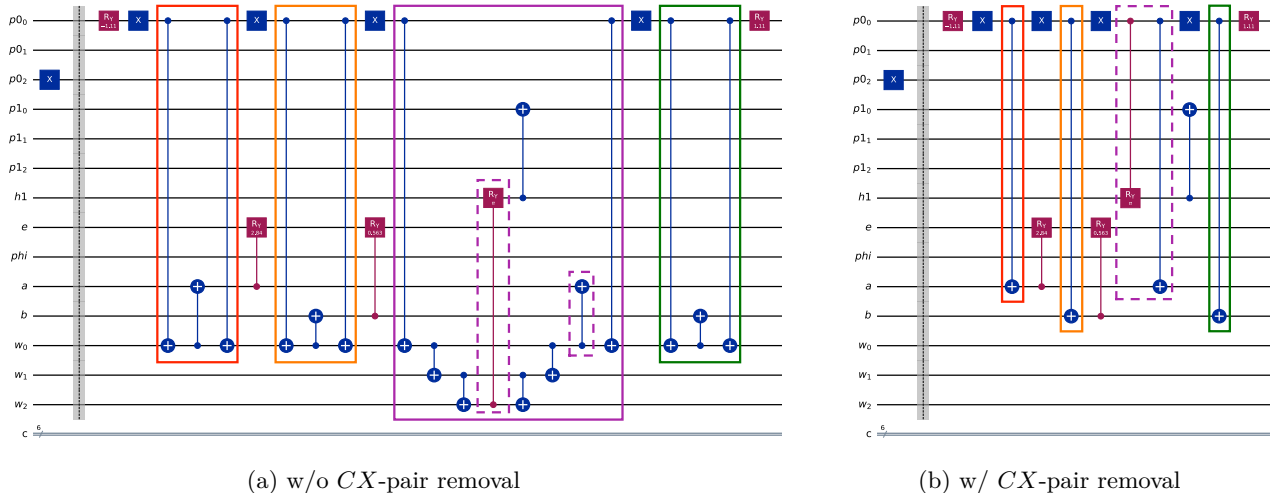


Figure 5: Optimized 1-step QPS circuit using AQCEL (a) w/o CX -pair removal and (b) w/ CX -pair removal. The colored boxes in the left figure show applicable parts of CX -pair removal, and the corresponding parts are shown in the same color in the right figure.

composed into two CX s and single-qubit gates here. The gate patterns highlighted by the colored boxes can be further reduced with AQCEL-v2 by applying the CX -pair removal, as shown in Figure 5(b), resulting in 11 CX s in total. The number of two-qubit gates and the fidelity for the 1-step QPS circuit are summarized in Table 1. The ideal topology corresponds to the case where all the qubits are connected to each other. The AQCEL-optimized circuits improve significantly both in gate counts and fidelity over Qiskit-only optimization, as already seen in Ref. [31]. Due to the improvements in gate errors on the hardware, the difference in fidelity between AQCEL-v1 and AQCEL-v2 is small with this size of circuits. Overall, the fidelity is much better than the result reported in [31] with the 27-qubit Falcon processor.

To evaluate the AQCEL performance against

	CX/CZ counts		Fidelity
	Ideal	<i>ibm_fez</i>	
Qiskit	115	246	0.46
AQCEL-v1	41 (23)	48 (24)	0.99 (0.96)
AQCEL-v2	25 (11)	36 (16)	0.99 (0.96)

Table 1: Number of two-qubit gates and the fidelity for the optimized 1-step QPS circuit on ideal topology with full connectivity and the *ibm_fez* backend. The optimization by AQCEL was performed with the noise threshold = 0.01 (0.05).

larger quantum circuit, we perform the same experiment for the 2-step QPS circuit. Figures 6 and 7 show the number of two-qubit gates for the optimized 2-step QPS circuit on the ideal topology with all-to-all connectivity and the *ibm_fez* backend, respectively. The number of two-qubit gates is reduced to 54% at the best with CX -pair removal on the ideal all-to-all connectivity. The fraction becomes moderate on the *ibm_fez* due to the additional CX gates introduced by the SWAP gates. Figure 8 shows the fidelities of the optimized circuits with the *ibm_fez* backend. With the CX -pair removal, the accumulated gate errors in AQCEL-v2 are expected to be reduced relative to AQCEL-v1, appearing as the improved fidelity at the thresholds below 0.15. The number of two-qubit gates is the maximum at the noise threshold around zero and decreases with increasing noise threshold (Figure 7). AQCEL identifies the computational bases of the control qubits above the threshold and decides what control operations can be removed based on the observed bitstrings. The higher the threshold becomes, the more reduction of the control operations occurs, hence the fidelity of the circuit as well. The improved fidelity for AQCEL-v2, reaching the maximum around the threshold of 0.15, indicates the trade-off between the reduction of gate errors and the decreased compatibility of the original and optimized circuits with increasing threshold. This supports the observation that the fidelity significantly decreases and there is no dif-

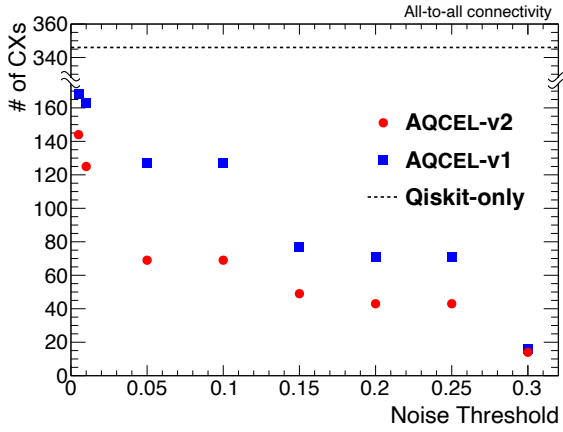


Figure 6: Number of CX s for the optimized 2-step QPS circuit as a function of noise threshold parameter in AQCEL. The red circles show AQCEL-v2, while the blue squares show AQCEL-v1. The black dotted line shows the Qiskit-only. The vertical axis is broken to highlight the AQCEL results, which are significantly smaller than the Qiskit-only results.

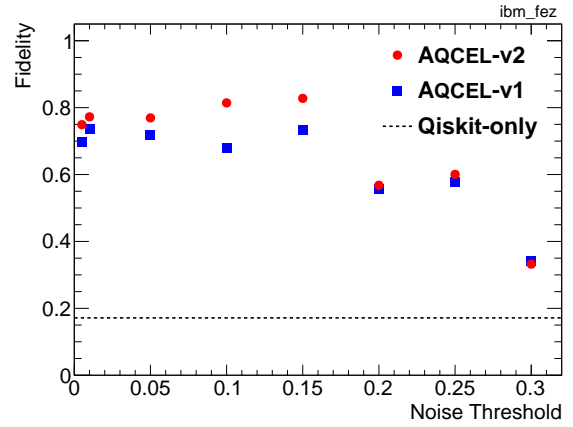


Figure 8: Hellinger fidelity between the distribution of bitstrings measured on the noiseless simulator for the 2-step QPS circuit and measured on the *ibm_fez* backend for the optimized circuit as a function of noise threshold parameter in AQCEL. The red circles show AQCEL-v2, while the blue squares show AQCEL-v1. The black dotted line shows the Qiskit-only.

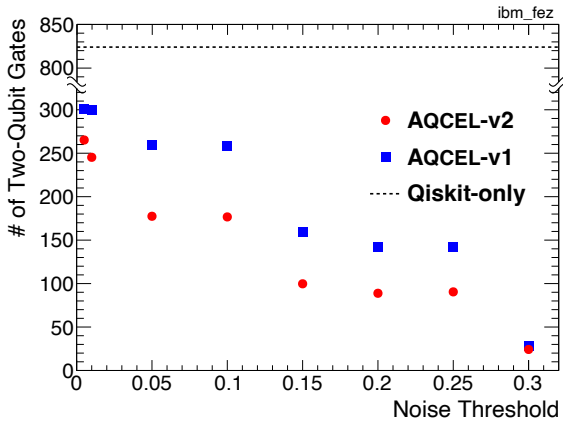


Figure 7: Number of two-qubit gates for the optimized 2-step QPS circuit on the *ibm_fez* backend as a function of noise threshold parameter in AQCEL. The red circles show AQCEL-v2, while the blue squares show AQCEL-v1. The black dotted line shows the Qiskit-only. The vertical axis is broken to highlight the AQCEL results, which are significantly smaller than the Qiskit-only results.

ference between AQCEL-v1 and AQCEL-v2 when the threshold becomes too high exceeding 0.15.

Figure 9 shows one of the physical observables: the distribution of the number of emissions per event for each configuration. The noise threshold in AQCEL is set to 0.15. Since this is a 2-step QPS circuit, the maximum number of emissions is two. We count the number of particles in the final state to calculate the emissions, but real quantum hardware sometimes returns unphysical re-

sults, i.e., zero particles in the final state, due to hardware noise. With Qiskit-only optimization, the shape of the emission distribution is significantly different from the ideal distribution obtained from the simulator, and 8% of the events have unphysical results. AQCEL-v2 returns the distribution closest to the ideal one. The largest discrepancy is observed between the ideal and the real hardware at the number of emissions = 1. This discrepancy with respect to the ideal is improved from +84% with AQCEL-v1 to +33% with AQCEL-v2.

Figure 10 shows the emission distribution for the 2-step QPS circuits with $g_{12} = 0$ and 1. The quantum circuits are optimized by AQCEL-v2 with the threshold = 0.15 and executed on the *ibm_fez* backend to compare with the noiseless simulator. The $g_{12} = 0$ means that there is no quantum interference effect between unobserved intermediate states in the showering processes. As shown in Figure 10, the measured distributions in real hardware reproduce the behavior of the true distributions with and without quantum interference. This result suggests that quantum computers are capable of calculating quantum interference effects, whose computational cost scales exponentially with the system size in classical simulations.

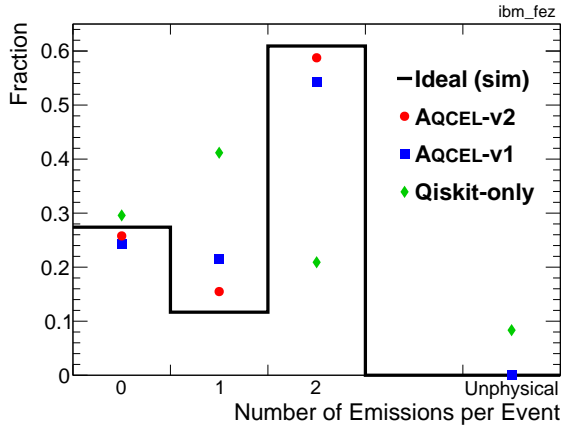


Figure 9: The number of emissions measured on the noiseless simulator and the *ibm_fez* backend for the 2-step QPS circuit. The black line shows the ideal distribution, the red circles show AQCEL-v2, the blue squares show AQCEL-v1, and the green diamonds show the Qiskit-only. The noise threshold parameter in AQCEL is set to 0.15.

6 Discussion

Implementing the state label manager allows us to reduce mis-optimization, especially in the low noise threshold region, and optimize efficiently if the states of control qubits are obviously identified. It is also expected that for qubits with a long idle time, we can suppress the effect of decoherence in the optimization by recording the states earlier in the circuit. The CX -pair removal helps remove unnecessary CX operators in the circuit, reducing the accumulated gate errors on the real hardware, and getting closer to the ideal results.

The AQCEL optimization protocol can be further improved in the future. Figure 11(a) shows a circuit for the two-qubit Grover's algorithm, and this circuit returns the state of $-|11\rangle$. The circuit shown in Figure 11(b) also outputs the same state of $-|11\rangle$ for the initial state of $|00\rangle$. This is an example circuit that can be optimized based on the initial states, but AQCEL-v2 cannot produce the optimized circuit like (b) from (a). This is because AQCEL-v2 does not support the X basis states of $|\pm\rangle = (|0\rangle \pm |1\rangle)/\sqrt{2}$. If the AQCEL is extended to deal with the $|\pm\rangle$ states and their entanglement with other qubits during the identification of unnecessary control operations, the circuit like this could be optimized, making the AQCEL more widely applicable.

We have demonstrated in this paper that AQCEL works well for the 2-step QPS circuit. For

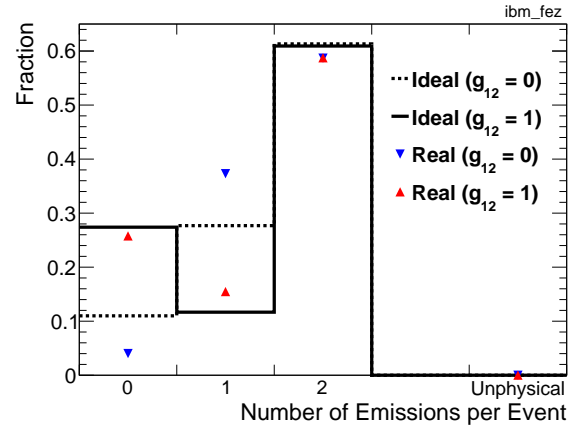


Figure 10: The number of emissions measured on the noiseless simulator and the *ibm_fez* backend for the 2-step QPS circuit with $g_{12} = 0$ and 1. The black dotted and solid lines show the ideal distribution for $g_{12} = 0$ and 1, respectively. The blue inverted triangles and red triangles show the distribution calculated by the *ibm_fez* backend for $g_{12} = 0$ and 1, respectively. The quantum circuits are optimized by AQCEL-v2 with the threshold = 0.15.

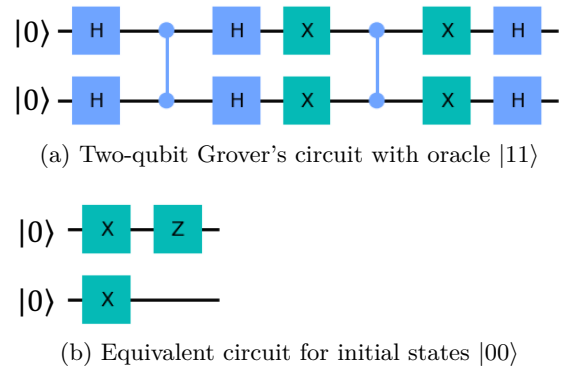


Figure 11: An example of the circuit that can be optimized based on initial states, whereas AQCEL cannot produce the optimized circuit at this moment.

the larger circuit, the AQCEL optimization is expected to work efficiently when the circuit depth is shallower, but do less efficiently with increasing circuit depth because the optimization based on measuring the computational basis states suffers from accumulated hardware noise. For a shallow quantum circuit, AQCEL should work effectively, no matter how many qubits are included in the circuit, because the AQCEL performs gate decomposition and measurements in polynomial time, independently of the qubit counts in the circuit. These features would provide the guidance for the future work.

7 Summary

In this paper, we have revisited AQCEL optimization protocol introduced in Ref. [31], the initial-state-dependent quantum circuit optimizer. AQCEL can detect and remove redundant control operations by constructing intermediate circuits and measuring the states of control qubits. In this work, the state label manager and the CX -pair removal have been introduced to bring performance improvements on top of the original features in [31]. The state label manager enables AQCEL to avoid unnecessary state measurements, reducing the required resources for optimization and preventing mis-optimization due to finite measurement shots and gate/readout errors. Recording the qubit states earlier in the circuit also helps reduce mis-optimization of the circuit caused by accumulated depolarizing errors. The CX -pair removal can eliminate unnecessary CX gates, most often produced by the decomposition of the multi-controlled operators and the redundant control operation removal.

To quantify the performance improvements, we have performed the 1-step and 2-step quantum parton shower simulation with AQCEL optimized circuits on a real IBM quantum processor. With the state label manager and the CX -pair removal, the number of two-qubit gates is reduced at best to 54% of the original AQCEL-optimized circuit. With these performance enhancements in AQCEL and hardware improvements in IBM quantum computer, we manage to achieve the Hellinger fidelity of 0.83 for the 2-step QPS circuit.

Acknowledgements

This work was supported by the Center of Innovation for Sustainable Quantum AI (JST Grant Number JPMJPF2221). We would like to thank Atsushi Matsuo and Toru Imai from IBM Quantum Japan for the discussions. We acknowledge the usage of IBM quantum computers for this work.

References

[1] Jay Chan, Wen Guan, Shaojun Sun, Alex Zeng Wang, Sau Lan Wu, Chen Zhou, Miron Livny, Federico Carminati, and Alberto Di Meglio. Application of Quantum

Machine Learning to High Energy Physics Analysis at LHC using IBM Quantum Computer Simulators and IBM Quantum Computer Hardware. *PoS, LeptonPhoton2019*: 049, 2019. DOI: [10.22323/1.367.0049](https://doi.org/10.22323/1.367.0049).

- [2] Koji Terashi, Michiru Kaneda, Tomoe Kishimoto, Masahiko Saito, Ryu Sawada, and Junichi Tanaka. Event Classification with Quantum Machine Learning in High-Energy Physics. *Comput Softw Big Sci*, 5:2, 2021. DOI: [10.1007/s41781-020-00047-7](https://doi.org/10.1007/s41781-020-00047-7).
- [3] Wen Guan, Gabriel Perdue, Arthur Pesah, Maria Schuld, Koji Terashi, Sofia Vallecorsa, and Jean-Roch Vlimant. Quantum machine learning in high energy physics. *Machine Learning: Science and Technology*, 2(1):011003, mar 2021. DOI: [10.1088/2632-2153/abc17d](https://doi.org/10.1088/2632-2153/abc17d). URL <https://dx.doi.org/10.1088/2632-2153/abc17d>.
- [4] Belis, Vasilis, González-Castillo, Samuel, Reissel, Christina, Vallecorsa, Sofia, Combarro, Elías F., Dissertori, Günther, and Reiter, Florentin. Higgs analysis with quantum classifiers. *EPJ Web Conf.*, 251:03070, 2021. DOI: [10.1051/epjconf/202125103070](https://doi.org/10.1051/epjconf/202125103070). URL <https://doi.org/10.1051/epjconf/202125103070>.
- [5] Tüysüz, Cenk, Carminati, Federico, Demirköz, Bilge, Dobos, Daniel, Fracas, Fabio, Novotny, Kristiane, Potamianos, Karolos, Vallecorsa, Sofia, and Vlimant, Jean-Roch. Particle track reconstruction with quantum algorithms. *EPJ Web Conf.*, 245:09013, 2020. DOI: [10.1051/epjconf/202024509013](https://doi.org/10.1051/epjconf/202024509013). URL <https://doi.org/10.1051/epjconf/202024509013>.
- [6] Annie Y. Wei, Preksha Naik, Aram W. Harrow, and Jesse Thaler. Quantum algorithms for jet clustering. *Phys. Rev. D*, 101:094015, May 2020. DOI: [10.1103/PhysRevD.101.094015](https://doi.org/10.1103/PhysRevD.101.094015). URL <https://link.aps.org/doi/10.1103/PhysRevD.101.094015>.
- [7] Benjamin Nachman, Davide Provasoli, Wibe A. de Jong, and Christian W. Bauer. Quantum algorithm for high energy physics simulations. *Phys. Rev. Lett.*, 126:062001, Feb 2021. DOI: [10.1103/PhysRevLett.126.062001](https://doi.org/10.1103/PhysRevLett.126.062001). URL <https://link.aps.org/doi/10.1103/PhysRevLett.126.062001>.

- [8] Christian W. Bauer, Zohreh Davoudi, A. Baha Balantekin, Tanmoy Bhattacharya, Marcela Carena, Wibe A. de Jong, Patrick Draper, Aida El-Khadra, Nate Gemelke, Masanori Hanada, Dmitri Kharzeev, Henry Lamm, Ying-Ying Li, Junyu Liu, Mikhail Lukin, Yannick Meurice, Christopher Monroe, Benjamin Nachman, Guido Pagano, John Preskill, Enrico Rinaldi, Alessandro Roggero, David I. Santiago, Martin J. Savage, Irfan Siddiqi, George Siopsis, David Van Zanten, Nathan Wiebe, Yukari Yamauchi, Kübra Yeter-Aydeniz, and Silvia Zorzetti. Quantum simulation for high-energy physics. *PRX Quantum*, 4:027001, May 2023. DOI: [10.1103/PRXQuantum.4.027001](https://doi.org/10.1103/PRXQuantum.4.027001). URL <https://link.aps.org/doi/10.1103/PRXQuantum.4.027001>.
- [9] C. A. Argüelles and B. J. P. Jones. Neutrino oscillations in a quantum processor. *Phys. Rev. Res.*, 1:033176, Dec 2019. DOI: [10.1103/PhysRevResearch.1.033176](https://doi.org/10.1103/PhysRevResearch.1.033176). URL <https://link.aps.org/doi/10.1103/PhysRevResearch.1.033176>.
- [10] Alberto Di Meglio, Karl Jansen, Ivano Tavernelli, Constantia Alexandrou, Srinivasan Arunachalam, Christian W. Bauer, Kerstin Borrás, Stefano Carrazza, Arianna Crippa, Vincent Croft, Roland de Putter, Andrea Delgado, Vedran Dunjko, Daniel J. Egger, Elias Fernández-Combarro, Elina Fuchs, Lena Funcke, Daniel González-Cuadra, Michele Grossi, Jad C. Halimeh, Zoë Holmes, Stefan Kühn, Denis Lacroix, Randy Lewis, Donatella Lucchesi, Miriam Lucio Martínez, Federico Meloni, Antonio Mezzacapo, Simone Montangero, Lento Nagano, Vincent R. Pascuzzi, Voica Radescu, Enrique Rico Ortega, Alessandro Roggero, Julian Schuhmacher, Joao Seixas, Pietro Silvi, Panagiotis Spentzouris, Francesco Tacchino, Kristan Temme, Koji Terashi, Jordi Tura, Cenk Tüysüz, Sofia Vallecorsa, Uwe-Jens Wiese, Shinjae Yoo, and Jinglei Zhang. Quantum computing for high-energy physics: State of the art and challenges. *PRX Quantum*, 5:037001, Aug 2024. DOI: [10.1103/PRXQuantum.5.037001](https://doi.org/10.1103/PRXQuantum.5.037001). URL <https://link.aps.org/doi/10.1103/PRXQuantum.5.037001>.
- [11] Roland C. Farrell, Ivan A. Chernyshev, Sarah J. M. Powell, Nikita A. Zemlevskiy, Marc Illa, and Martin J. Savage. Preparations for quantum simulations of quantum chromodynamics in 1+1 dimensions. i. axial gauge. *Phys. Rev. D*, 107:054512, Mar 2023. DOI: [10.1103/PhysRevD.107.054512](https://doi.org/10.1103/PhysRevD.107.054512). URL <https://link.aps.org/doi/10.1103/PhysRevD.107.054512>.
- [12] Anthony Ciavarella, Natalie Klco, and Martin J. Savage. Trailhead for quantum simulation of su(3) yang-mills lattice gauge theory in the local multiplet basis. *Phys. Rev. D*, 103:094501, May 2021. DOI: [10.1103/PhysRevD.103.094501](https://doi.org/10.1103/PhysRevD.103.094501). URL <https://link.aps.org/doi/10.1103/PhysRevD.103.094501>.
- [13] Ali Javadi-Abhari, Matthew Treinish, Kevin Krsulich, Christopher J. Wood, Jake Lishman, Julien Gacon, Simon Martiel, Paul D. Nation, Lev S. Bishop, Andrew W. Cross, Blake R. Johnson, and Jay M. Gambetta. Quantum computing with Qiskit, 2024.
- [14] Ed Younis, Costin C Iancu, Wim Lavrijsen, Marc Davis, Ethan Smith, and US-DOE. Berkeley quantum synthesis toolkit (bqskit) v1, 04 2021. URL <https://www.osti.gov/biblio/1785933>.
- [15] Ji Liu, Luciano Bello, and Huiyang Zhou. Relaxed peephole optimization: A novel compiler optimization for quantum circuits, 2020. URL <https://arxiv.org/abs/2012.07711>.
- [16] Bob Coecke and Ross Duncan. Interacting quantum observables: categorical algebra and diagrammatics. *New Journal of Physics*, 13(4):043016, apr 2011. DOI: [10.1088/1367-2630/13/4/043016](https://doi.org/10.1088/1367-2630/13/4/043016). URL <https://dx.doi.org/10.1088/1367-2630/13/4/043016>.
- [17] Bob Coecke. Basic zx-calculus for students and professionals, 2023. URL <https://arxiv.org/abs/2303.03163>.
- [18] Robert R. Tucci. An introduction to cartan’s kak decomposition for qc programmers, 2005. URL <https://arxiv.org/abs/quant-ph/0507171>.
- [19] V.V. Shende, S.S. Bullock, and I.L. Markov. Synthesis of quantum-logic circuits. *IEEE Transactions on Computer-Aided Design of Integrated Circuits and Systems*, 25(6):1000–1010, 2006. DOI: [10.1109/TCAD.2005.855930](https://doi.org/10.1109/TCAD.2005.855930).

- [20] Henry Zou, Matthew Treinish, Kevin Hartman, Alexander Ivrii, and Jake Lishman. Lightsabre: A lightweight and enhanced sabre algorithm, 2024. URL <https://arxiv.org/abs/2409.08368>.
- [21] Albert T. Schmitz, Nicolas P. D. Sawaya, Sonika Johri, and A. Y. Matsuura. Graph optimization perspective for low-depth trotter-suzuki decomposition, 2023. URL <https://arxiv.org/abs/2103.08602>.
- [22] Jennifer Paykin, Albert T. Schmitz, Mohannad Ibrahim, Xin-Chuan Wu, and A. Y. Matsuura. Pcoast: A pauli-based quantum circuit optimization framework, 2023. URL <https://arxiv.org/abs/2305.10966>.
- [23] Lorenza Viola, Emanuel Knill, and Seth Lloyd. Dynamical decoupling of open quantum systems. *Phys. Rev. Lett.*, 82:2417–2421, Mar 1999. DOI: [10.1103/PhysRevLett.82.2417](https://doi.org/10.1103/PhysRevLett.82.2417). URL <https://link.aps.org/doi/10.1103/PhysRevLett.82.2417>.
- [24] Zhenyu Cai, Ryan Babbush, Simon C. Benjamin, Suguru Endo, William J. Huggins, Ying Li, Jarrod R. McClean, and Thomas E. O’Brien. Quantum error mitigation. *Rev. Mod. Phys.*, 95:045005, Dec 2023. DOI: [10.1103/RevModPhys.95.045005](https://doi.org/10.1103/RevModPhys.95.045005). URL <https://link.aps.org/doi/10.1103/RevModPhys.95.045005>.
- [25] Yasunari Suzuki, Suguru Endo, Keisuke Fujii, and Yuuki Tokunaga. Quantum error mitigation as a universal error reduction technique: Applications from the nisq to the fault-tolerant quantum computing eras. *PRX Quantum*, 3:010345, Mar 2022. DOI: [10.1103/PRXQuantum.3.010345](https://doi.org/10.1103/PRXQuantum.3.010345). URL <https://link.aps.org/doi/10.1103/PRXQuantum.3.010345>.
- [26] Andre He, Benjamin Nachman, Wibe A. de Jong, and Christian W. Bauer. Zero-noise extrapolation for quantum-gate error mitigation with identity insertions. *Phys. Rev. A*, 102:012426, Jul 2020. DOI: [10.1103/PhysRevA.102.012426](https://doi.org/10.1103/PhysRevA.102.012426). URL <https://link.aps.org/doi/10.1103/PhysRevA.102.012426>.
- [27] Kristan Temme, Sergey Bravyi, and Jay M. Gambetta. Error mitigation for short-depth quantum circuits. *Phys. Rev. Lett.*, 119:180509, Nov 2017. DOI: [10.1103/PhysRevLett.119.180509](https://doi.org/10.1103/PhysRevLett.119.180509). URL <https://link.aps.org/doi/10.1103/PhysRevLett.119.180509>.
- [28] Akel Hashim, Ravi K. Naik, Alexis Morvan, Jean-Loup Ville, Bradley Mitchell, John Mark Kreikebaum, Marc Davis, Ethan Smith, Costin Iancu, Kevin P. O’Brien, Ian Hincks, Joel J. Wallman, Joseph Emerson, and Irfan Siddiqi. Randomized compiling for scalable quantum computing on a noisy superconducting quantum processor. *Phys. Rev. X*, 11:041039, Nov 2021. DOI: [10.1103/PhysRevX.11.041039](https://doi.org/10.1103/PhysRevX.11.041039). URL <https://link.aps.org/doi/10.1103/PhysRevX.11.041039>.
- [29] Paul D. Nation, Hwajung Kang, Neereja Sundaresan, and Jay M. Gambetta. Scalable mitigation of measurement errors on quantum computers. *PRX Quantum*, 2:040326, Nov 2021. DOI: [10.1103/PRXQuantum.2.040326](https://doi.org/10.1103/PRXQuantum.2.040326). URL <https://link.aps.org/doi/10.1103/PRXQuantum.2.040326>.
- [30] Joel J. Wallman and Joseph Emerson. Noise tailoring for scalable quantum computation via randomized compiling. *Phys. Rev. A*, 94:052325, Nov 2016. DOI: [10.1103/PhysRevA.94.052325](https://doi.org/10.1103/PhysRevA.94.052325). URL <https://link.aps.org/doi/10.1103/PhysRevA.94.052325>.
- [31] Wonho Jang, Koji Terashi, Masahiko Saito, Christian W. Bauer, Benjamin Nachman, Yutaro Iiyama, Ryunosuke Okubo, and Ryu Sawada. Initial-State Dependent Optimization of Controlled Gate Operations with Quantum Computer. *Quantum*, 6:798, September 2022. ISSN 2521-327X. DOI: [10.22331/q-2022-09-08-798](https://doi.org/10.22331/q-2022-09-08-798). URL <https://doi.org/10.22331/q-2022-09-08-798>.
- [32] Adriano Barenco, Charles H. Bennett, Richard Cleve, David P. DiVincenzo, Norman Margolus, Peter Shor, Tycho Sleator, John A. Smolin, and Harald Weinfurter. Elementary gates for quantum computation. *Phys. Rev. A*, 52:3457–3467, Nov 1995. DOI: [10.1103/PhysRevA.52.3457](https://doi.org/10.1103/PhysRevA.52.3457). URL <https://link.aps.org/doi/10.1103/PhysRevA.52.3457>.
- [33] Plato Deliyannis, James Sud, Diana Chamaki, Zoë Webb-Mack, Christian W. Bauer, and Benjamin Nachman. Improving quantum simulation efficiency of final state radiation with dynamic quantum circuits. *Phys. Rev. D*, 106:036007, Aug 2022.

DOI: 10.1103/PhysRevD.106.036007. URL
[https://link.aps.org/doi/10.1103/
PhysRevD.106.036007](https://link.aps.org/doi/10.1103/PhysRevD.106.036007).

- [34] See Supplemental Material at [http://link.aps.org/supplemental/10.1103/
PhysRevLett.126.062001](http://link.aps.org/supplemental/10.1103/PhysRevLett.126.062001) for details of the QPS quantum algorithm.
- [35] Guido Van Rossum and Fred L. Drake. *Python 3 Reference Manual*. CreateSpace, Scotts Valley, CA, 2009. ISBN 1441412697.